THE EUROPEAN
PHYSICAL JOURNAL D

Regular Article - Molecular Physics and Chemical Physics

A cluster source for photoelectron spectroscopy in VUV and X-ray ranges

Chiara Nicolafrancesco[1,2], Sebastian Hartweg[1], Jean-Francois Gil[1], Emmanuel Robert[1], Jean-Marc Ramillon[2], Christophe Nicolas[1], Suvasthika Indrajith[2], John Bozek[1], Laurent Nahon[1], Aleksandar R. Milosavljević[1,a], and Patrick Rousseau[2]

[1] Synchrotron SOLEIL, L'Orme des Merisiers, St Aubin, BP 48, 91192 Gif sur Yvette Cedex, France
[2] Normandie Univ, ENSICAEN, UNICAEN, CEA, CNRS, CIMAP, 14000 Caen, France

Abstract. A detailed description of a custom-made gas aggregation cluster source is given as well as of its coupling to permanent molecular beam end-stations of the beamlines DESIRS and PLEIADES at the French national facility synchrotron SOLEIL. Using (hydrated) hypoxanthine clusters as a case study, the production of clusters with different source parameters is discussed based on Vacuum Ultra-Violet (VUV) mass spectrometry. The ability of the cluster source to perform photoelectron spectroscopy is illustrated by photoelectron spectra obtained for valence and core shells.

1 Introduction

Clusters made by aggregation of atoms or molecules are intermediate states of matter in between the gas phase and the condensed matter. Their physico-chemical properties differ from both the isolated atom/molecule, as some inter-atomic/inter-molecular interactions may already occur, and from the bulk material due to their finite size. Therefore, it is of particular interest from fundamental and applied points of view to probe these sub-nanometric/nanometric size-specific properties. More specifically, in a biological/biomimetic context, inter-molecular interactions are responsible for the formation of DNA-bases pairs [1]. Gas phase offers an ideal solvent- and substrate-free environment to study such specific inter-molecular interactions. Moreover, in the context of radiation damage, clusters of biomolecules can mimic a simple chemical environment in the gas phase, thus allowing to address the effect of the environment on the ionisation/excitation and on the subsequent decay processes [2,3]. For biomolecular isolated molecules as well as clusters, a further step consists in considering micro-hydration by the production of mixed biomolecule-water clusters [4–8]. Finally, clusters of biomolecules are a reservoir of matter with a well-controlled size and nuclear geometries, very suitable for the study of intra-cluster reactivity leading to the formation of covalent species such as polypeptides via radiation [9] or collisional excitation [10,11].

Valence- and core-level spectroscopy associated with the tunable light provided by synchrotron radiation is a widely used and universal technique to probe electronic and molecular structures of matter [12,13]. While photoelectron emission allows probing the occupied states, available unoccupied states are revealed by photoabsorption spectroscopy. Considering systems of biological interest, photoelectron spectroscopy (PES), angular resolved PES (ARPES), X-ray photoelectron spectroscopy (XPS), and near-edge X-ray absorption fine structure (NEXAFS) spectroscopy have been widely performed on relatively small isolated elementary bricks of life brought in the gas phase by resistive-heating [14–16] as well as by aerosol thermodesorption [17,18]. Using electrospray ionisation, it is possible to bring in the gas phase much larger biopolymers whose structure and dynamics have been also studied in a wide photon energy range from Vacuum Ultra-Violet (VUV) to X-rays [19,20]. Due to the limited density of these large biomolecular ions, their trapping is required and thus among the aforementioned spectroscopies only VUV absorption/action spectroscopy and NEXAFS can be performed [20,21] which are much less informative than PES. Note that the investigation of isolated building blocks is not sufficient to understand complex biopolymers such as proteins and DNA, because intermolecular interactions between their building blocks and nearby solvent molecules, involving non-covalent hydrogen bonds and van der Waals interactions [22–24], play a very important role in defining their structure and function.

Gas-phase PES and XPS allow to investigate the electronic structure and dynamics of bare and hydrated biomolecular clusters, compare their properties to both those of a single molecule and a condensed molecular film, and then use theoretical modelling to shed

[a] e-mail: milosavljevic@synchrotron-soleil.fr (corresponding author)

light onto the effects of weak intermolecular interactions [25]. To perform such an experimental research, one needs a controllable cluster source coupled to the versatile spectroscopic set-ups that exist at modern synchrotron facilities. In this work, we have employed a custom-made gas aggregation cluster source coupled to the beamlines DESIRS [26] and PLEIADES [27] at the French national synchrotron facility SOLEIL. Here, we give a detailed description of the cluster source and its coupling to the existing permanent molecular beam chambers available at these two beamlines. The production of (hydrated) clusters of hypoxanthine, a purine derivative, is discussed based on VUV mass spectrometry measurements. Finally, in order to illustrate the performance of the present devices, photoelectron spectra obtained from both the valence and core shells are given.

2 Experimental details

2.1 Cluster source

The present source relies on the gas aggregation cluster formation. Such cluster sources allow the formation of rather large clusters, for instance metal clusters of several 10000s of atoms can be produced [28]. Moreover, they are versatile, and different molecular clusters types can be produced such as Van der Waals bonded clusters of fullerenes [29,30] and of polycyclic aromatic hydrocarbons [31,32], or H-bonded clusters of water [33,34] and of (hydrated) biomolecules [35,36].

In a gas aggregation source, the growth of cluster occurs by addition of vaporised atoms/molecules in a few mbar of inert gas [37], similar to the formation process of smokes or clouds. When a cluster grows by collision of two particles (atoms, molecules or smaller clusters), an excess of energy is due to the binding formation energy. Usually, in cluster sources this energy is taken away in three body collisions where the third body is a particle from the buffer gas, typically a rare gas (He, Ar). Apart from three body collisions, a cluster source needs to fulfil a second condition, namely the formation of cold enough clusters in order to avoid their dissociation/evaporation. This is particularly critical in the case of molecular clusters as their typical binding energy is below 1 eV. Therefore, in a gas aggregation cluster source, the cluster formation occurs in the so-called condensation channel, usually a double-walled pipe allowing the circulation of liquid nitrogen (LN$_2$). There, the vapour made of a mixture of the buffer gas and the vaporised particles reaches a thermal equilibrium by the numerous collisions of the buffer gas atoms with the LN$_2$-cold walls of the condensation channel. Flowing the buffer gas (typically few hundreds of mL.min^{-1}) through the gas aggregation cluster source also allows conveying the clusters outside the source. Note that an alternative cooling method relies on adiabatic expansion to form the cold clusters [23,38–40]. Also, there are several other approaches such as

cluster sources relying on pickup by inert gas nanodroplets [41,42], or desorption from liquid droplets [43] or aerosols ([44]. Nevertheless, description of all these techniques is out of the scope of the present paper.

The present cluster source, named CELENO for Cluster ELEctroN emissiOn (in French, Celeno is one of the Pleiades sisters), is based on the one developed by Bergen et al. [45] and adapted from the original one by Brechignac et al. [46]. A scheme of the CELENO source is drawn in Fig. 1. The main component of the source is a stainless steel chamber (diameter = 140 mm, height = 90 mm) placed under vacuum. From one side, the chamber is drilled to allow for the gas line of the buffer gas introduction, on the opposite side sits the condensation channel and in between an oven produces the atomic/molecular vapour. The buffer gas flow is regulated by a mass flow controller (Brooks SLA5850). The typical pressure of He measured by a capacitive gauge (Leybold CERAVAC CTR100) in the stainless steel chamber is about 10 mbar, and the typical flow is about 150-200 mL.min^{-1}. The sample powder is placed in a resistively heated oven. It consists of a 3 cm^3 capacity stainless steel cylindrical reservoir opened at one end and wrapped by a wire heating element. The condensation channel is an 82.5 mm long cylinder, with a 12 mm diameter aperture on the oven side, and a 2.2 mm diameter one on the interaction chamber side. It is cooled down by a double-walled LN$_2$ circulation line.

In a gas aggregation cluster source, several parameters control the conditions inside the condensation channel where the cluster growth occurs [28]. By increasing the oven temperature, one increases the vapour pressure of the sample and thus the amount of matter available to grow clusters. The buffer gas pressure allows controlling the number of collisions in the condensation channel. It has been shown that the nature of the buffer gas plays a role, the heavier and more polarisable the buffer gas, the larger the energy transfer; therefore, Ar is preferred to He if one looks for the production of the largest clusters [28]. Finally, one can control the condensation channel itself by varying its length or temperature [28]. With the present source, it is not possible to change the length of the channel and it is difficult to regulate a temperature higher than the LN$_2$ one. In the present work, we used He as the buffer gas, allowing the formation of clusters containing tens of molecules and thus an efficient detection/identification, whereas larger clusters are out of the scope of the present study. Therefore in practice, we controlled the cluster production by varying two parameters: the oven temperature and the buffer gas flow.

In order to produce hydrated clusters, we follow the method introduced by Kocisek et al. [47]. It relies on the humidification of the carrier gas before its injection into the cluster source. Thus, we insert a small closed cup containing ultra-pure water along the gas line upstream the mass flow controller as shown in Fig. 1. The He buffer gas flows inside a Nafion tube (Perma Pure) immersed in water. Nafion membrane possesses a water-selective permeability. Therefore, water molecules pass
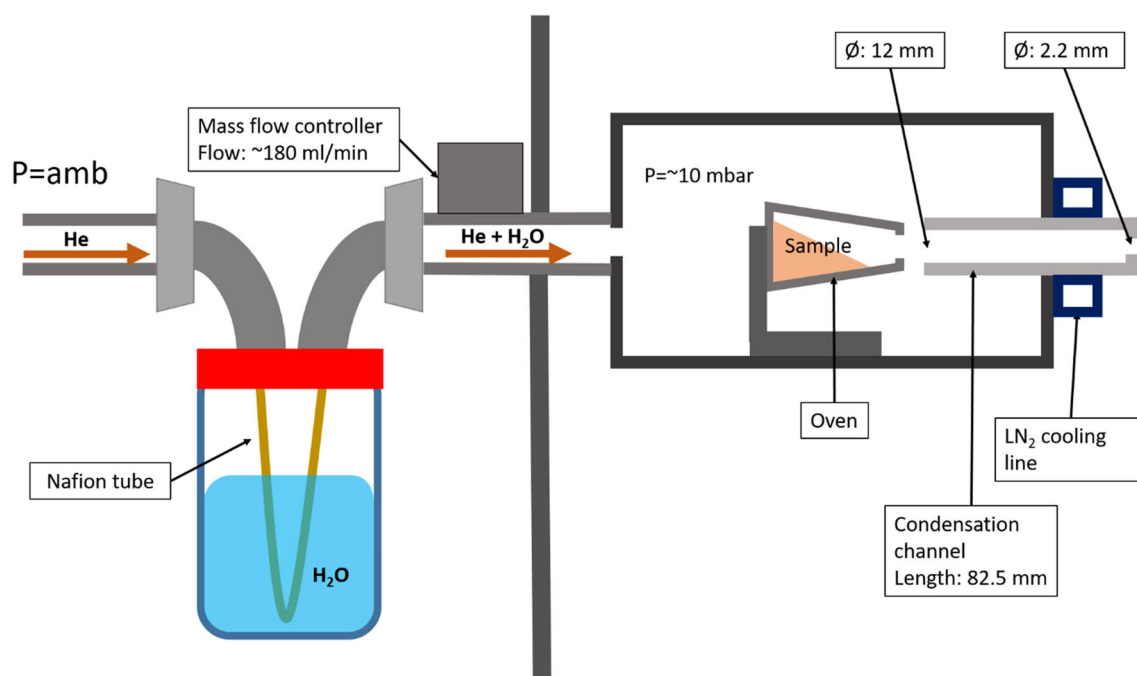
Fig. 1 Schematic representation of the CELENO gas aggregation cluster source, equipped to produce hydrated clusters. The cluster source chamber has a diameter of 140 mm and a height of 90 mm

though the tube wall to be mixed with the He buffer gas and transported to the cluster chamber. The humidification of the buffer gas is proportional to the surface of the Nafion membrane in contact with water: the larger the area, the larger the number of water molecules that will be transported in the cluster chamber by the buffer gas, as discussed further below.

2.2 Coupling to the DESIRS beamline

The DESIRS beamline provides intense VUV radiation of fully controllable linear or circular polarisation in the 4-40 eV photon energy range [26]. The photon beam is produced by a versatile electromagnetic undulator whose high harmonics are efficiently removed by using a gas filter [26] prior to the 6-m normal incidence monochromator equipped with various gratings ensuring a tailored flux/resolution compromise. In the present work, we chose a moderate resolution ($\sim$ 10 meV at 10 eV), ensuring a rather high flux (in the few 10^{12} photons.sec^{-1} range). The CELENO cluster source described above has been coupled to the permanent molecular beam chamber SAPHIRS [48] equipped with the double imaging photoelectron/photoion coincidence (i^{2}PEPICO) spectrometer DELICIOUS 3 [49], permanently installed on branch A of the beamline.

The DELICIOUS 3 spectrometer allows coincident detection of photoions and photoelectrons produced by each given photoionisation event. Photoelectrons are detected via a velocity map imaging (VMI) spectrometer, allowing determining their kinetic energy- and angular distributions after Abel inversion of the images. The ion side of the spectrometer consists of a mod-

ified Wiley–McLaren time-of-flight mass spectrometer providing accurate ion mass information, and featuring additional lenses to allow for the determination of ion kinetic energy releases (IKER, not used in the scope of this work). The photoions are extracted perpendicularly to the direction of the neutral molecular or cluster beam. A deflector electrode in the ion flight tube is used to ascertain that also heavy ions with a large initial momentum in the direction of the molecular beam do not miss the 40 mm MCP detector. Therefore, the most significant contribution to the mass dependence represents the detection efficiency of the MCP detector that is known to decrease for increasing masses. In the DELICIOUS, 3 spectrometer ions are accelerated to $\sim$ 3800 eV. In this kinetic energy range the channel efficiency decreases between masses of 100 amu and $\sim$ 3000 amu by about a factor of 2, according to Fraser [50]. The coincidence detection scheme allows filtering of the electron VMI data according to ion mass and spatial region of interest (ROI) on the ion detector. The latter allows an additional separation of background signals arising from impurities in the $10^{-8} - 10^{-6}$ mbar working vacuum from genuine signals corresponding to species of interest originating from the molecular beam. Provided that cascading processes are neglected, or known, this set-up allows to perform ARPES on size-selected clusters [38]. Even when the cascading processes are not fully controllable/known, it is possible to select very cold nascent clusters [51], discarding hot high KER-related ones, to the detriment of the signal level.

The SAPHIRS molecular beam chamber features a two skimmer double differentially pumped stage. The CELENO cluster source, placed in the source cham-
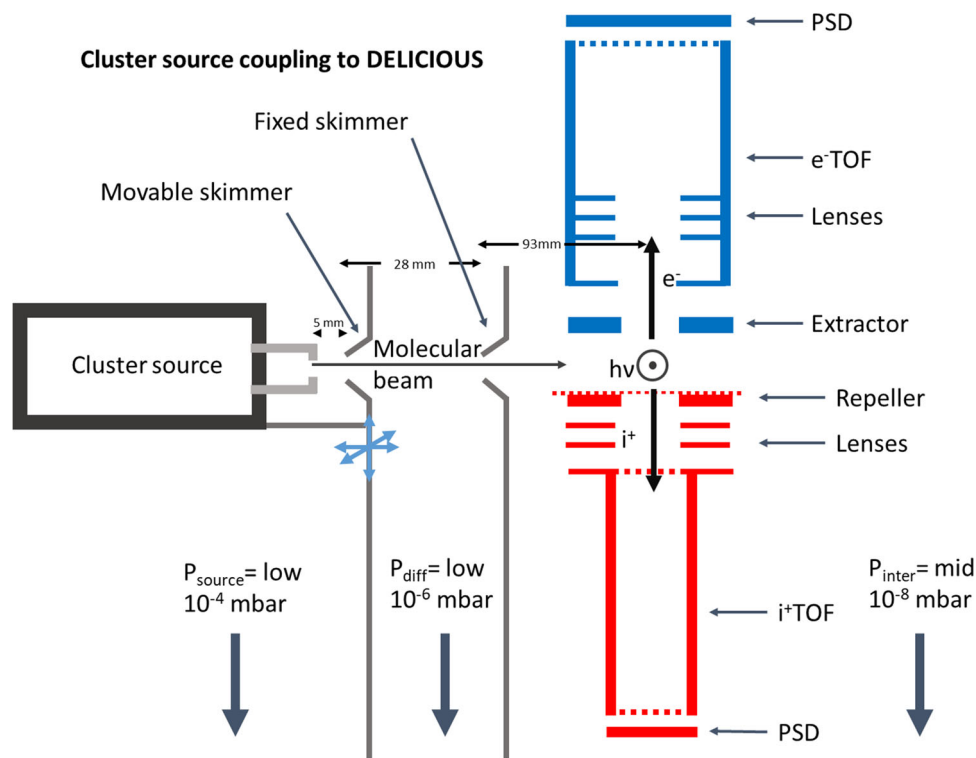
Fig. 2 Schematic description of the coupling of the CELENO source to the SAPHIRS molecular beam chamber equipped with the DELICIOUS 3 double imaging electron/ion coincidence spectrometer (the electron side on the top, ion side down) at DESIRS beamline. PSD stands for position sensitive detector. The pumping speeds on the DESIRS set-up are 3000 l/s in the jet chamber (2000 l/s +1000 l/s), 900 l/s (3x300 l/s) in the differential chamber, and 2000 l/s (2x1000 l/s) in the ionisation chamber

ber, is fixed to the first skimmer holder (Fig. 2), which is mounted onto a motorised 3-axis translational stage allowing the mechanical alignment of the first skimmer attached to the cluster source with respect to the second skimmer and the ionisation region. A fixed distance of 5 mm was chosen between the exit of the cluster source and the first skimmer, providing a compromise between creating sufficient cluster density at the ionisation region and avoiding clogging of the first skimmer with deposited sample molecules. The second skimmer, placed at $\sim$ 28 mm from the first one, is fixed spatially relative to the ionisation region, located 93 mm downstream from the tip of the second skimmer. Under typical working conditions, the pressure in the SAPHIRS source chamber is about 10^{-4} mbar, causing only a small pressure rise in the differential pumping stage (10^{-6} mbar), and only a vanishing pressure rise in the spectrometer chamber (mid 10^{-8} mbar)

By performing i^{2}PEPICO spectroscopy in the VUV photon range, we were able to study both the mass-distribution of the produced clusters, to benchmark the source, as well as to measure the electrons angle and energy distribution (ARPES), emitted by photoionisation of the mass-selected or full-mass distribution clusters. In the context of the present article, the essentially background-free ROI-filtered mass spectra of the clusters produced by the CELENO provided us with important information on cluster size distributions and, in

the case of the hydrated clusters, the number of water molecules attached to them, *i.e.* the degree of solvation.

2.3 Coupling to the PLEIADES beamline

The photon source for the PLEIADES beamline used in the present experiment is a permanent magnet APPLE II type undulator, with a period of 80 mm, in combination with a high-flux, 600 lines/mm grating of the modified Petersen plane grating monochromator [27]. In order to measure the X-ray photoelectron spectra of aggregated targets, we employed the VG Scienta R4000 hemispherical electron energy analyser end-station coupled to the multi-purpose source chamber (MPSC) [52]. The CELENO cluster source was installed inside the MPSC (Fig. 3). Compared to the coupling of the cluster source to DESIRS described above, there is no differential pumping stage. The pressure in the MPSC is kept at high 10^{-5} mbar. The working pressure in the ionisation chamber is typically in the range of high 10^{-6} mbar to low 10^{-5} mbar, with a base pressure in 10^{-8} mbar.

The source can be moved close to the interaction zone, through a metallic tube belonging to the MPSC chamber, ended by a skimmer and entering inside the ionisation vacuum chamber hosting the Scienta spectrometer, close to the interaction region. In the present
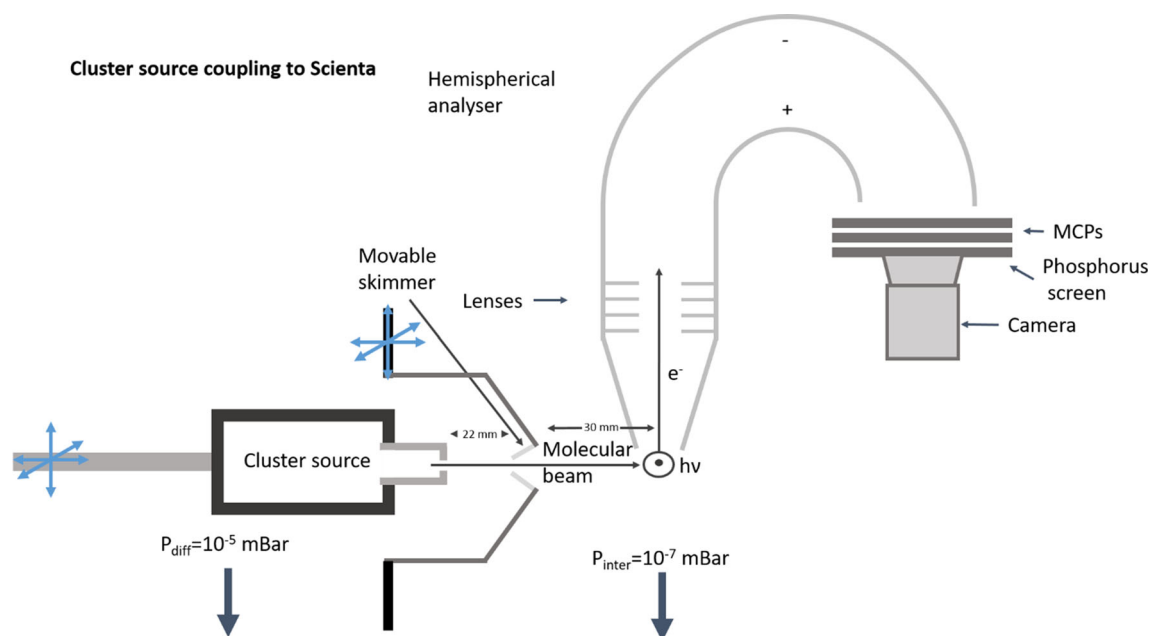
Fig. 3 Schematic description of the coupling of the CELENO source to the hemispherical energy analyser for photoelectron spectroscopy at PLEIADES. The pumping speeds on the PLEIADES set-up are 5300 l/s (2x2650 l/s) in the MPSC chamber hosting the cluster source and 1100 l/s (800 l/s +300 l/s) in the ionisation chamber

experiment, the distance between the cluster source and the skimmer was set at 22 mm. The exit of the cluster source can be moved on the X and Y axes with respect to the exit skimmer. The skimmer can be also independently moved on the X and Y axes, in order to guarantee an alignment between the molecular beam and the photon beam [52]. The distance between the skimmer and the photon beam is 30 mm. The interaction chamber can be moved perpendicularly to the cluster beam direction, in order to align the interaction region with the Scienta analyser entrance lens.

3 Results and discussion

The CELENO cluster source has been coupled to VUV and soft X-ray synchrotron radiation in order to study the photoelectron spectroscopy of (hydrated) hypoxanthine clusters. Here we present results on the production of (hydrated) clusters of hypoxanthine with the present gas aggregation cluster source. By tuning the cluster source parameters, we can change the clusters size distribution as observed in VUV mass spectrometry. Finally, we illustrate the performance of the present device to record photoelectron spectra of both valence and core shells.

3.1 Influence of the source parameters on the production of hypoxanthine clusters

Hypoxanthine is a purine derivative, as guanine and adenine, with brute formula $C_5H_4N_4O$ (mass 136 u)

thus differing from adenine by oxidative deamination of one of the C atoms. We used a pure commercial sample (Sigma-Aldrich, 99% purity) without further purification.

As mentioned before, with the design of the CELENO source, the parameters controlling the cluster size distribution are the He buffer gas flow (He_{flow}) and the associated pressure (He_p) inside the cluster source condensation channel, and the vapour pressure of hypoxanthine that is controlled by the oven temperature (T_{oven}), and the condensation channel temperature (T_{cc}) [28]. During the experiments, we kept the T_{cc} constant at the LN_2 temperature, while tuning the other two parameters: He_{flow} and T_{oven}. However, it should be noted that these parameters are not independent. Indeed, by increasing the He flow, the number of collisions with the oven walls increases leading the oven to cool down. Therefore, a variation of the buffer gas flow always induces a variation of the oven temperature, which can be compensated for by adjusting the heating current if a constant T_{oven} is desired.

ROI-filtered VUV mass spectra recorded at the photon energy of 9.5 eV are shown in Fig. 4 for different cluster source conditions. The general distribution of the cluster sizes follows a log-normal trend, and the observed distribution differs in its maximum and width with the cluster source parameters. The observed clusters correspond mostly to ionised cationic species $(Hyp)_n^+$. However, the deviation from the expected isotopic contribution due to ^{13}C in larger clusters indicates that protonation also occurs for larger species as shown in the inset of Fig. 4b, and thus, a minor partial dissociation of the clusters occurs in the current ionisation conditions. Additional experiments performed with

a photon energy of 12.1 eV clearly indicates a much more pronounced protonation of the species observed. H-bonded clusters dissociation through a proton transfer is a very efficient way to dissipate energy, thus following ionisation above the threshold the dissociation of H-bonded clusters will give protonated species. In the case of mixed clusters of inert gas and H-bonded molecules, the release of the inert gas atoms can lead to the formation of radical cation clusters of water besides the formation of both deprotonated and protonated clusters [53]. Therefore, the observation of protonated species is usually associated with cluster dissociation. Nevertheless, as the protonation signal is rather weak for a photon energy of 9.5 eV and that the distribution observed follow a log-normal trend, we can assume that the fragmentation of the cluster is mostly quenched and thus that the observed size distribution reflects quite well the initial size distribution in the current ionisation conditions. Note that the detection efficiency of larger clusters is somewhat reduced due to their lower velocity impact on the microchannel plates (see Experimental details); therefore, the real size distribution is slightly shifted towards larger sizes. However, in the present study, we compare the size distribution as a function of the source parameters and thus the observed relative changes in the distributions reflect the changes. The secondary peak observed after the dimer peak in Fig. 4 panels c) is due to some residual gas pollution of the interaction chamber. In these cases, the separation of background signals via ROI-filtering is incomplete, since we applied a deflection voltage in order to detect larger clusters more efficiently. Finally, a general observation of the mass spectra also evidences secondary peaks shifted by 18 u in the case of larger clusters. Hydrated clusters are thus also produced in the present conditions even without hydration of the buffer gas. Indeed, an incomplete flushing of the gas line most probably explains the hydration observed. This also explains the increased hydration observed when increasing $\mathrm{He_{flow}}$ comparing Figs. 4c and 4d. After further pumping of the gas line, we do not observe any more these secondary peaks.

We now consider the variation of the cluster distribution with the CELENO source parameters. In Fig. 4a, the source parameters were 491 K for the oven temperature and 180 mL.min^{-1} for the buffer gas flow. The log-normal distribution has a maximum corresponding to the pentamer (m/z = 680), and the observed maximal cluster size corresponds to $n \sim 15$ molecules. The signals associated with the hypoxanthine molecule and with its dimer are rather intense in these source conditions. Their relative intensities decreased when increasing the oven temperature from 491 K to 498 K (Fig. 4b) and to 505 K (Fig. 4c). The monomer is not visible in the mass spectrum recorded at the latter temperature. Note that the ionisation energy of the hypoxanthine monomer is 8.85 eV [54], well below 9.5 eV, so should be detected if they are present in the molecular beam. In fact, as clusters are growing by addition of monomer and dimers, the free monomers and dimers observed at lower temperature are aggregating with larger species
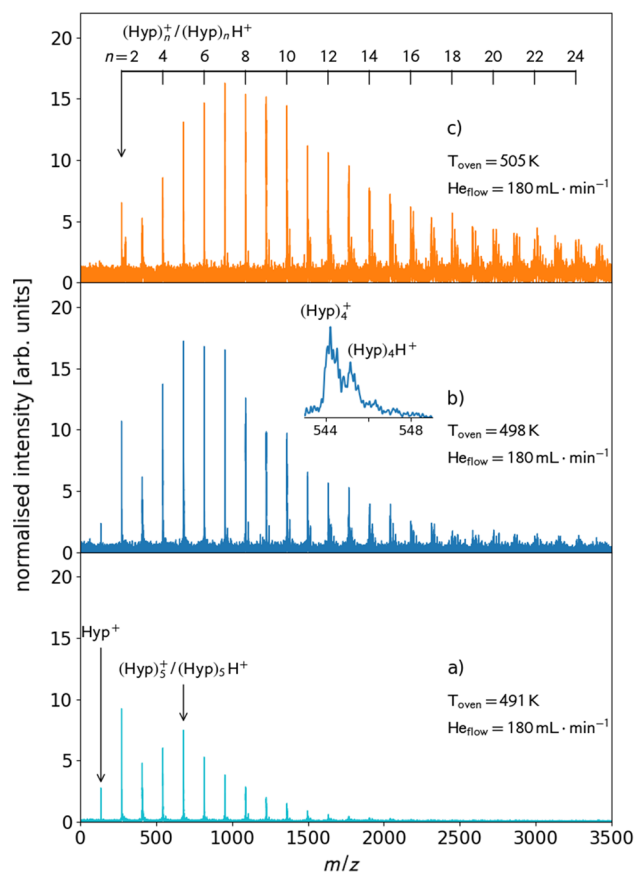

Fig. 4 VUV photoionisation mass spectra of hypoxanthine clusters obtained at the photon energy of 9.5 eV with different cluster source parameters. The intensity is normalised to the acquisition time

at higher temperature due to an increased density of material to form clusters. Considering the Clausius–Clapeyron equation and thermochemical properties of hypoxanthine [39], the vapour pressures at 491 K and 498 K correspond, respectively, to about 33% and 58 % of the one at the temperature of 505 K. Accordingly, keeping the $\mathrm{He_{flow}}$ constant and increasing the oven temperature to 498 K, the distribution of clusters shifts towards larger sizes as shown in Fig. 4b. The log-normal distribution has now a rather flat maximum for the cluster size between the pentamer (m/z = 680) and the heptamer (m/z = 952), and the relative intensity of the larger clusters increases allowing the observation of clusters made of more than 20 hypoxanthine molecules. In Fig. 4c where the oven temperature has been increased to 505 K, we clearly notice a further shift of the cluster size distribution towards higher m/z. The log-normal distribution has now a flat maximum for the cluster size between the hexamer (m/z = 816) and the decamer (m/z = 1360) and even higher relative intensities for the larger cluster sizes. Moreover, the values of the intensity being normalised to the acquisition time thus reflect an increasing count rates with temperature, meaning that we produce more clusters when increasing the oven temperature.

To conclude, variations of the He flow and of the oven temperature affect the cluster distribution and we can control the size distribution by carefully controlling the gas aggregation source parameters as shown previously [28,45,46]. It is noteworthy that a small variation of the oven temperature drastically affects the cluster distributions as usually the vapour pressure varies quickly with the temperature in this range [28,45,46].

3.2 Production of hydrated hypoxanthine clusters

As described above, the production of hydrated clusters relies on a Nafion membrane. He gas flowing inside the Nafion tube will be humidified depending on the surface of the tube immersed in water. Thus, the regulation of the hydration level of clusters is possible by variation of the surface of the Nafion tube in contact with liquid water.

In Fig. 5, we can observe how different levels of humidification of the buffer gas can affect the cluster formation and distribution. First, we consider the mass spectrum collected with the Nafion tube submerged in ultra-pure water, as displayed in Fig. 5a. Here, up to two water molecules are attached to the monomer. Starting from the dimer (m/z = 272), the hydration level rises up to nine added water molecules. The relative intensity of the hydrated species compared to the bare clusters increases with the number of hypoxanthine molecules, as does the maximum number of water molecules attached to a given hypoxanthine cluster. From the hexamer, the intensity of the signal of the pure hypoxanthine cluster becomes similar to the one of the hydrated clusters. This makes an accurate description more complex, as mass peaks start to overlap with each other. On the other hand, when the Nafion was just touching the water surface (Fig. 5b), we could see that only one water molecule could be added to the monomer. The level of hydration is reduced for all cluster sizes, for instance up to seven water molecules can be added to the dimer compared to nine in the previous hydration conditions. In conclusion, the hydration of the buffer gas through a Nafion membrane is an efficient way to produce hydrated clusters. The level of hydration can be controlled by adjusting the surface of the membrane in contact with water.

3.3 Photoelectron spectroscopy of pure hypoxanthine clusters

Finally to illustrate the performance of the coupling of the CELENO source to DESIRS and PLEIADES beamlines, we present here some typical photoelectron spectra obtained in the VUV and X-ray ranges. It should be noted that due to different vacuum systems (pumping speed, presence of differential pumping stages) at the two beamlines PLEIADES and DESIRS, the buffer gas pressure instead of the buffer gas flow needs to be considered if one wants to compare the cluster size distributions obtained.
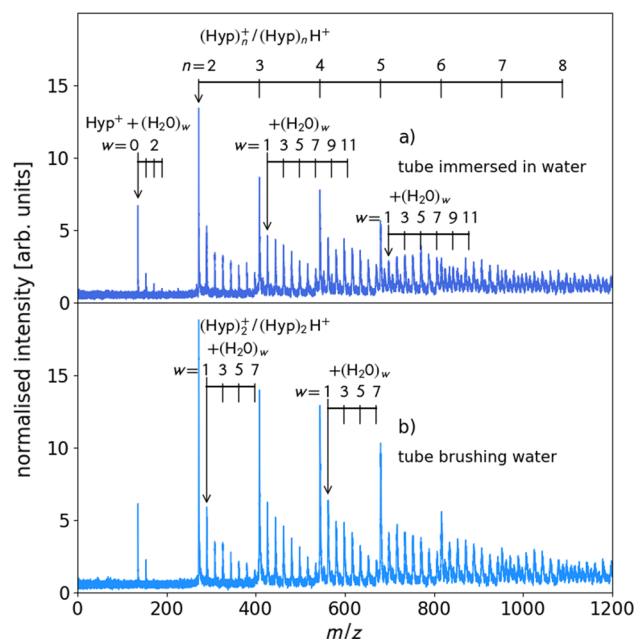

Fig. 5 VUV photoionisation mass spectra obtained at the photon energy of 9.5 eV with different hydration levels of the buffer gas. The intensity is normalised to the acquisition time

A valence photoelectron spectrum of hypoxanthine clusters obtained with 11 eV photons and summed up over all observed cluster sizes from the monomer to the octamer is presented in Fig. 6. The acquisition time for this spectrum was four hours allowing for satisfactory statistics. We notice the same spectral features as observed for the photoionisation of the isolated molecule of hypoxanthine [54]. However, in the case of the clusters, the features are broader and they appear shifted towards lower binding energy as expected. A detailed analysis of the cluster mass-resolved photoelectron spectra is beyond the scope of the present article, and will be the subject of a forthcoming complete report.

A XPS spectrum around the carbon 1s edge recorded at the photon energy of 370 eV is shown in Fig. 7. The overall spectral resolution was about 0.55 eV, defined by the photon energy resolution of 0.4 eV (for the monochromator exit slit of 200 μm) and the Scienta analyser resolution of 0.375 eV (for the slit width of 1.5 mm and pass energy of 100 eV). The acquisition time was about two hours, resulting in about 300 counts in the peak maximum, with respect to the background. The XPS peaks corresponding to different hypoxanthine carbon atoms appear less separated with respect to the previously published spectrum for a single hypoxanthine molecule [55], which is due to both a binding energy shift towards lower values and a spectral broadening induced by aggregation, as already noticed for uracil clusters [25]. However, a more detailed analysis will be given in a forthcoming publication.
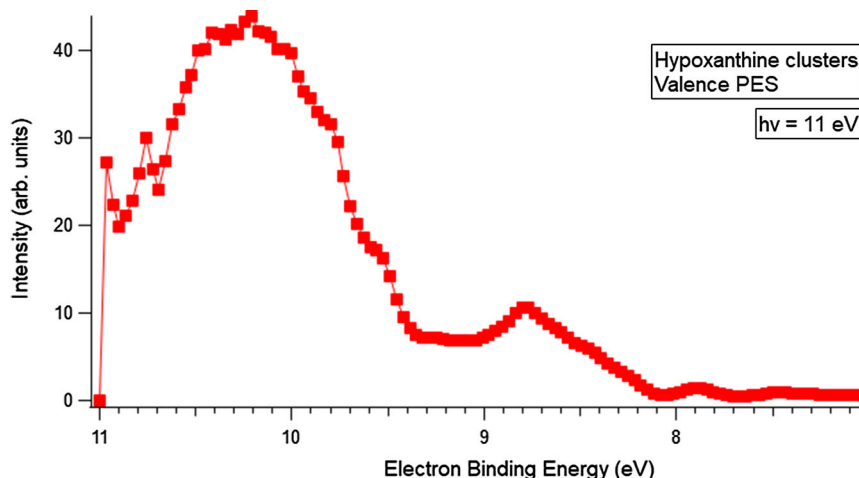
Fig. 6 Valence photoelectron spectrum obtained for a photon energy of 11 eV and summed up over the different hypoxanthine clusters. The cluster source oven temperature was $T_{oven} = 498$ K, and the He buffer gas flow and pressure were $He_{flow} = 180$ mL.min^{-1} and $He_p = 12.3$ mbar
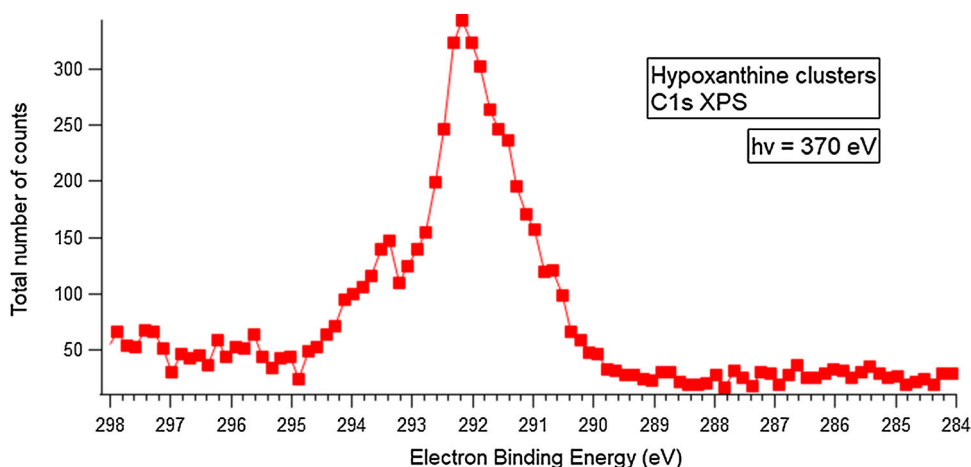

Fig. 7 Carbon 1s X-ray photoelectron spectrum of hypoxanthine clusters recorded at a photon energy of c.a. 370 eV, recorded during about 2 hours. The cluster source oven temperature was $T_{oven} = 481$ K, and the He buffer gas flow and pressure were $He_{flow} = 180$ mL.min^{-1} and $He_p = 18$ mbar. The binding energy scale is calibrated according to the C1s ionisation potential of CO_2 [56].

4 Conclusions

A gas aggregation cluster source has been developed to perform state-of-the-art synchrotron-based photoelectron spectroscopy in the VUV and X-ray ranges. It has been successfully coupled to the DELICIOUS 3 double imaging photoelectron photoion coincidence spectrometer at the DESIRS beamline of SOLEIL and to the Scienta hemispherical energy analyser at the PLEIADES beamline of SOLEIL. As a case study, we have considered (hydrated) clusters of hypoxanthine. Using VUV photoionisation time-of-flight mass spectrometry, we have studied the produced cluster size distribution as a function of the source conditions. We have shown that in the case of the bare clusters, their size distribution depends on the buffer gas flow and the oven temperature. The latter cluster size distribution

study on DESIRS may provide only an estimation of the one used on PLEIADES for given source parameters, due to different experimental configurations and pumping efficiencies. Further work will be therefore performed to determine more accurately cluster sizes in the XPS measurements. We also produced hydrated clusters of hypoxanthine by humidification of the buffer gas through a Nafion membrane. The level of hydration of clusters can be modified and controlled by adjusting the surface of tube immersed in water. Finally, we were able to obtain photoelectron spectra within a reasonable acquisition time. The experimental work presented here paves the way towards investigation of different bio-molecular clusters.

cal staff of SOLEIL for running smoothly the facility under projects 20191563 and 20191936.

Author contributions

PR and ARM designed the experiments. JFG, ER, and JMR designed the mechanical parts. CN, SH, LN, SI, ChrN, JB, PR, and ARM performed the experiments. CN and SH analysed the data. CN, SH, LN, PR, and ARM prepared the draft manuscript. All authors commented the draft manuscript and approved the final manuscript.

Data Availability Statement This manuscript has no associated data, or the data will not be deposited. [Authors comment: The datasets generated during and/or analysed during the current study are available from the corresponding author on reasonable request.]

References

1. A. Abo-Riziq, L. Grace, E. Nir, M. Kabelac, P. Hobza, M.S. De Vries, Proc. Natl. Acad. Sci. U.S.A. **102**, 20 (2005)
2. T. Schlathölter, F. Alvarado, S. Bari, A. Lecointre, R. Hoekstra, V. Bernigaud, B. Manil, J. Rangama, B. Huber, ChemPhysChem **7**, 2339 (2006)
3. S. Maclot, M. Capron, R. Maisonny, A. Lawicki, A. Méry, J. Rangama, J.Y. Chesnel, S. Bari, R. Hoekstra, T. Schlathölter, B. Manil, L. Adoui, P. Rousseau, B.A. Huber, ChemPhysChem **12**, 930 (2011)
4. S.K. Kim, W. Lee, D.R. Herschbach, J. Phys. Chem. **100**, 7933 (1996)
5. A. Domaracka, M. Capron, S. Maclot, J.Y. Chesnel, A. Méry, J.C. Poully, J. Rangama, L. Adoui, P. Rousseau, B.A. Huber ,Phys. Conf. Ser. **373**, 012005 (2012)
6. B. Barc, M. Ryszka, J. Spurrell, M. Dampc, P. Limão-Vieira, R. Parajuli, N.J. Mason, S. Eden, J. Chem. Phys. **139**, 244311 (2013)
7. M. Neustetter, J. Aysina, F.F. Da Silva, S. Denifl, Angew. Chemie—Int. Ed. **54**, 9124 (2015)
8. E. Wang, X. Ren, W.Y. Baek, H. Rabus, T. Pfeifer, A. Dorn, Nat. Commun. **11**, 2194 (2020)
9. S. Lee, S.J. Valentine, J.P. Reilly, D.E. Clemmer, J. Am. Chem. Soc. **133**, 15834 (2011)
10. M. Nihamkin, A. Isaak, A. Albeck, Y. Mastai, Y. Toker, J. Phys. Chem. Lett. **10**, 10100 (2020)
11. P. Rousseau, D.G. Piekarski, M. Capron, A. Domaracka, L. Adoui, F. Martín, M. Alcamí, S. Díaz-Tendero, B.A. Huber, Nat. Commun. **11**, 3818 (2020)
12. S. Hüfner, *Photoelectron Spectroscopy—-Principles and Applications* (Springer, Berlin, 2003)
13. J. Stöhr, R. Gomer, *NEXAFS Spectroscsopy* (Springer, Berlin, 1992)
14. Martin Schwell, M. Hochlaf, Top. Curr. Chem. **355**, 155 (2014)
15. K.C. Prince, P. Bolognesi, V. Feyer, O. Plekan, L. Avaldi, J. Electron Spectros. Relat. Phenomena **204**, 335 (2015)
16. P. Bolognesi, L. Avaldi, in Photoprocesses with Biomolecules in the Gas Phase in Nanoscale Insights into Ion-Beam Cancer Therapy, ed. by A.V. Solov'yov (Springer International Publishing, Berlin, 2017), p. 209
17. F. Gaie-Levrel, G. A. Garcia, M. Schwell, L. Nahon
18. M. Tia, B. Cunha De Miranda, S. Daly, F. Gaie-Levrel, G.A. Garcia, L. Nahon, I. Powis, J. Phys. Chem. A **118**, 2765 (2014)
19. A. Giuliani, A.R. Milosavljevic, F. Canon, L. Nahon, Mass Spectrom. Rev. **33**, 424 (2014)
20. A.R. Milosavljevic, A. Giuliani, C. Nicolas, Gas-Phase Near-Edge X-Ray Absorption Fine Structure (NEXAFS) Spectroscopy of Nanoparticles, Biopolymers, and Ionic Species in X-ray and Neutron Techniques for Nanomaterials Characterization, ed. by C.S.S.R. Kumar (Springer, Berlin, 2016), p. 451
21. S. Bari, D. Egorov, T.L.C. Jansen, R. Boll, R. Hoekstra, S. Techert, V. Zamudio-Bayer, C. Bülow, R. Lindblad, G. Leistner, A. Lawicki, K. Hirsch, P.S. Miedema, B. von Issendorff, J.T. Lau, T. Schlathölter, Chem. —A Eur. J. **24**, 7631 (2018)
22. O. Björneholm, G. Öhrwall, M. Tchaplyguine, Nucl. Instr. Methods Phys. Res. Sect. A Accel. Spectrometers, Detect. Assoc. Equip. **601**, 161 (2009)
23. M. Ahmed, O. Kostko, Phys. Chem. Chem. Phys. **22**, 2713 (2020)
24. A. Karshikoff, Non-Covalent Interactions in Proteins (Imperial College Press, London, 2006)
25. G. Mattioli, L. Avaldi, P. Bolognesi, J.D. Bozek, M.C. Castrovilli, J. Chiarinelli, A. Domaracka, S. Indrajith, S. Maclot, A.R. Milosavljevic, C. Nicolafrancesco, C. Nicolas, P. Rousseau, Sci. Rep. **10**, 13081 (2020)
26. L. Nahon, N. De Oliveira, G.A. Garcia, J.F. Gil, B. Pilette, O. Marcouillé, B. Lagarde, F. Polack, J. Synchrotron Radiat. **19**, 508 (2012)
27. Synchrotron SOLEIL, PLEIADES beamline (2021). https://www.synchrotronsoleil.fr/en/beamlines/pleiades. Accessed 31 Mar 2021
28. U. Zimmermann, N. Malinowski, U. Näher, S. Frank, T.P. Martin, Z. Phys. D **31**,85(1994)
29. K. Hansen, R. Muller, H. Hohmann, E.E.B. Campbell, Z. Phys. D **40**, 361 (1997)
30. B. Manil, L. Maunoury, B.A. Huber, J. Jensen, H.T. Schmidt, H. Zettergren, H. Cederquist, S. Tomita, P. Hvelplund, Phys. Rev. Lett. **91**, 215504 (2003)
31. M. Schmidt, A. Masson, C. Bréchignac, Int. J. Mass Spectrom. **252**, 173 (2006)
32. P. Rousseau, A. Lawicki, A.I.S. Holm, M. Capron, R. Maisonny, S. MacLot, E. Lattouf, H.A.B. Johansson, F. Seitz, A. Méry, J. Rangama, H. Zettergren, S. Rosén, H.T. Schmidt, J.Y. Chesnel, A. Domaracka, B. Manil, L. Adoui, H. Cederquist, B.A. Huber, Nucl. Instr. Methods Phys. Res. Sect. B Beam Interact. with Mater. Atoms **279**, 140 (2012)
33. S. Zamith, P. Labastie, J.M. Lhermite, J. Chem. Phys. **136**, 214301 (2012)
34. R. Maisonny, M. Capron, S. Maclot, J.C. Poully, A. Domaracka, A. Méry, L. Adoui, P. Rousseau, B.A. Huber In: J. Phys. Conf. Ser. **438**, 012007 (2013)
35. P. Markush, P. Bolognesi, A. Cartoni, P. Rousseau, S. Maclot, R. Delaunay, A. Domaracka, J. Kocisek, M.C. Castrovilli, B.A. Huber, L. Avaldi, Phys. Chem. Chem. Phys. **18**, 16721 (2016)

36. I. Braud, S. Zamith, J. Cuny, L. Zheng, J.M. L'Hermite, J. Chem. Phys. **150**, 014303 (2019)
37. H. Haberland, *Clusters of Atoms and Molecules* (Springer, Berlin, 1994)
38. S. Hartweg, B.L. Yoder, G.A. Garcia, L. Nahon, R. Signorell, Phys. Rev. Lett. **118**, 103402 (2017)
39. T.E. Gartmann, S. Hartweg, L. Ban, E. Chasovskikh, B.L. Yoder, R. Signorell, Phys. Chem. Chem. Phys. **20**, 16364 (2018)
40. C. Joblin, L. Dontot, G.A. Garcia, F. Spiegelman, M. Rapacioli, L. Nahon, P. Parneix, T. Pino, P. Bréchignac, J. Phys. Chem. Lett. **8**, 3697 (2017)
41. A. Mauracher, O. Echt, A.M. Ellis, S. Yang, D.K. Bohme, J. Postler, A. Kaiser, S. Denifl, P. Scheier, Phys. Rep. **751**, 1 (2018)
42. M. Fárník, J. Fedor, J. Kočišek, J. Lengyel, E. Pluharová, V. Poterya, A. Pysanenko, Phys. Chem. Chem. Phys. **23**, 3195 (2021)
43. K. Kitajima, T. Majima, T. Nishio, Y. Oonishi, S. Mizutani, J.ya Kohno, M. Saito, H. Tsuchida, Nucl. Instr. Methods Phys. Res. Sect. B Beam Interact. with Mater. Atoms **424**, 10 (2018)
44. J. Zahardis, S. Geddes, G.A. Petrucci, Anal. Chem. **83**, 2409 (2011)
45. T. Bergen, X. Biquard, A. Brenac, F. Chandezon, B.A. Huber, D. Jalabert, H. Lebius, M. Maurel, E. Monnand, J. Opitz, A. Pesnelle, B. Pras, C. Ristori, J.C. Rocco, Rev. Sci. Instrum. **70**, 3244 (1999)
46. C. Bréchignac, P. Cahuzac, F. Carlier, M. de Frutos, A. Masson, J. Roux, Z. Phys. D**19**, 195 (1991)
47. J. Kočišek, A. Pysanenko, M. Fárník, J. Fedor, J. Phys. Chem. Lett. **7**, 3401 (2016)
48. X. Tang, G.A. Garcia, J.F. Gil, L. Nahon, Rev. Sci. Instrum. **86**, 123108 (2015)
49. G.A. Garcia, B.K. Cunha De Miranda, M. Tia, S. Daly, L. Nahon, Rev. Sci. Instrum. **84**, 053112 (2013)
50. G.W. Fraser, Int. J. Mass Spectrom. **215**, 13 (2002)
51. M. Tia, Ph.D. thesis, Université Paris-Sud (2014)
52. A. Lindblad, J. Söderström, C. Nicolas, E. Robert, C. Miron, Rev. Sci. Instrum. **84**, 113105 (2013)
53. R.T. Jongma, Y. Huang, S. Shi, A.M. Wodtke, J. Phys. Chem. A **102**, 8847 (1998)
54. V. Feyer, O. Plekan, R. Richter, M. Coreno, K.C. Prince, Chem. Phys. **358**, 33 (2009)
55. O. Plekan, V. Feyer, R. Richter, A. Moise, M. Coreno, K.C. Prince, I.L. Zaytseva, T.E. Moskovskaya, D.Y. Soshnikov, A.B. Trofimov, J. Phys. Chem. A **116**, 5653 (2012)
56. V. Myrseth, J.D. Bozek, E. Kukk, L.J. Sathre, T.D. Thomas, J. Electron Spectros. Relat. Phenomena **122**, 57 (2002)